


Phylogeography and population differentiation in the *Psittacanthus calyculatus* (Loranthaceae) mistletoe: a complex scenario of climate–volcanism interaction along the Trans-Mexican Volcanic Belt

María José Pérez-Crespo¹ | Juan Francisco Ornelas¹  | Antonio González-Rodríguez² | Eduardo Ruiz-Sánchez³ | Antonio Acini Vásquez-Aguilar¹ | Santiago Ramírez-Barahona¹

¹Departamento de Biología Evolutiva, Instituto de Ecología AC, Xalapa, Veracruz, Mexico

²Laboratorio de Genética de la Conservación, Instituto de Investigaciones en Ecosistemas y Sustentabilidad (IIES), UNAM, Morelia, Michoacán, Mexico

³Escuela Nacional de Estudios Superiores Unidad Morelia (UNAM), Morelia, Michoacán, Mexico

Correspondence

Juan Francisco Ornelas, Departamento de Biología Evolutiva, Instituto de Ecología, AC, Xalapa, Veracruz, México.
Email: francisco.ornelas@inecol.mx

Funding information

Consejo Nacional de Ciencia y Tecnología, Grant/Award Number: 61710, 155686, 365006/248109, 155686; Departamento de Biología Evolutiva, Instituto de Ecología, AC, Grant/Award Number: 20030/10563

Editor: Alain Vanderpoorten

Abstract

Aim: The formation of the Trans-Mexican Volcanic Belt (TMVB) played an important role in driving inter- and intraspecific diversification at high elevations. However, Pleistocene climate changes and ecological factors might also contribute to plant genetic structuring along the volcanic belt. Here, we analysed phylogeographical patterns of the parrot-mistletoe *Psittacanthus calyculatus* to determine the relative contribution of these different factors.

Location: Trans-Mexican Volcanic Belt.

Methods: Using nuclear and chloroplast DNA sequence data for 370 individuals, we investigate the genetic differentiation of 35 populations across the species range. We conducted phylogenetic, population and spatial genetic analyses of *P. calyculatus* sequences along with ecological niche modelling and Bayesian inference methods to gain insight into the structuring of genetic variation of these populations.

Results: Our analyses revealed population structure with three genetic groups corresponding to individuals from Oaxaca and those from the central-eastern and western TMVB regions. A significant genetic signal of demographic expansion, an east-to-west expansion predicted by species distribution modelling, and approximate Bayesian computation analyses strongly supported a scenario of habitat isolation and invasion of TMVB by *P. calyculatus* during the late-Pleistocene.

Main conclusions: The genetic differentiation of *P. calyculatus* may be explained by the combined effects of (1) geographical isolation linked to the effects of the glacial/interglacial cycles and environmental factors, driving genetic differentiation from congeners into more xeric vegetation and (2) the invasion of TMVB from east to west, suggesting a role for both colonization and glacial/interglacial cycles models.

KEYWORDS

Loranthaceae, Mesoamerica, Mexico, mistletoes, phylogeography, Pleistocene, *Psittacanthus*, Trans-Mexican Volcanic Belt

1 | INTRODUCTION

The geological development of the Trans-Mexican Volcanic Belt (TMVB), a magmatic arc of c. 8,000 volcanic structures, had a profound impact as a biogeographical barrier between Nearctic and Neotropical biotas (Halffter, 1987). The formation of the TMVB is divided into four episodes: (1) the early to mid-Miocene arc formation (19–8 Ma), (2) a late Miocene episode of eastward migrating volcanism (11–3 Ma), (3) very late Miocene to early Pliocene volcanism (7.5–3 Ma), and (4) late Pliocene to Quaternary arc formation (3.5 Ma–Holocene; Ferrari, Orozco-Esquivel, Manea, & Manea, 2012; Gómez-Tuena, Orozco-Esquivel, & Ferrari, 2007). The final episode was characterized by the construction of large stratovolcanoes during the last 1.5 Myr, some of which are still active (Ferrari et al., 2012; Gómez-Tuena et al., 2007), and it coincided with the dramatic climate fluctuations of the Pleistocene (Mastretta-Yanes, Moreno-Letelier, Piñero, Jorgensen, & Emerson, 2015). Five periods of ice cap advances are identified for volcanoes in the central TMVB (Vázquez-Selem & Heine, 2011), including the Nexcoalango advance at 195 ka in which glaciers reached 3,000 m above sea level. There were four pulses of glacial maxima between 20 and 7 ka, with glaciers reaching 3,400–4,000 m (Vázquez-Selem & Heine, 2011). The impact of these glaciations on the distribution of TMVB taxa was probably not as dramatic as that observed at more northerly latitudes; however, during Pleistocene glacial advances, mean annual temperatures between 3,000 and 4,000 m above sea level were 5–9°C lower than at present (12–5°C), the timberline shifted to 700–900 m below its present position (from 5,000 m to 3,800–4,000 m), and most extensions of pine–oak forest shifted downward by 730–930 m, from 4,000 to 3,000 m (Caballero, Lozano-García, Vázquez-Selem, & Ortega, 2010; Lozano-García, Sosa-Nájera, Sugiura, & Caballero, 2005; Vázquez-Selem & Heine, 2011).

Phylogeographical studies have indicated that the uplift of the TMVB played an important role in driving inter- and intraspecific diversification along or across the volcanic belt in plants (Mastretta-Yanes et al., 2014; Ruiz-Sanchez & Ornelas, 2014; Ruiz-Sanchez & Specht, 2013) and vertebrates (Bryson, García-Vázquez, & Riddle, 2011; Kingston et al., 2014; McCormack, Heled, Delaney, Peterson, & Knowles, 2011; Parra-Olea, Windfield, Velo-Antón, & Zamudio, 2012; Rodríguez-Gómez & Ornelas, 2015; Velo-Antón, Parra, Parra-Olea, & Zamudio, 2013). The age of genetic patterns reported for the region temporally fall across the range from the Miocene-Pliocene (e.g. Ruiz-Sanchez & Specht, 2013) to Pleistocene (e.g. McCormack et al., 2011). In the case of the latter, since volcanoes in the TMVB are < 1.5 Myr old (Ferrari et al., 2012), the patterns might be the result of Miocene-Pliocene landscape configurations (Ornelas, González, Espinosa de los Monteros, Rodríguez-Gómez, & García-Feria, 2014), Pleistocene climate fluctuations (McCormack et al., 2011), and/or more recent volcanism (Mastretta-Yanes et al., 2015). The potentially synergistic effect of volcanic activity during the last episode of the TMVB formation and Plio-Pleistocene climatic

changes on the distribution of genetic variation needs further investigation (Mastretta-Yanes et al., 2015).

The aim of this study was to investigate the relative contribution of historical and contemporary climate–volcanism interaction along the TMVB in shaping phylogeographical diversity in *Psittacanthus calyculatus* (DC.) G. Don, 1834 (Loranthaceae), a mistletoe characteristic of temperate forest edges. This hemiparasite of trees is likely to have tracked host range changes linked to Pleistocene climate events (e.g. Ornelas et al., 2016). The first three episodes of evolution of the TMVB (Ferrari et al., 2012) formed highlands where populations could have differentiated allopatrically, generating an east–west differentiation of sister lineages (Mastretta-Yanes et al., 2015; Figure 1). The emergence of more recent intermediate volcanoes created continuous highlands that might have facilitated either colonization and admixture from differentiated east–west sources (fragmentation model) or stepping-stone east-to-west colonization and interglacial differentiation (colonization model). Glacial advances might have resulted in secondary contact of populations isolated during interglacial cycles, leading to admixture and gene flow and erasing earlier patterns of genetic structuring (glacial/interglacial cycles model; Figure 1).

In this article, we examine nuclear and chloroplast DNA sequence variation to explain genetic diversity in *P. calyculatus*. Specifically, we test the following hypotheses: (1) the genetic differentiation in *P. calyculatus* was pre-Pleistocene in origin, concordant with the first three episodes of the TMVB formation, (2) that the Miocene east–west division of the TMVB was a long-standing barrier to dispersal that separated groups of populations, and (3) that further genetic differentiation occurred in response to changes in the distribution of habitats during Pleistocene glacial/interglacial cycles. We aim to test these hypotheses by using an integrative analytical approach that includes phylogenetic, population, and spatial genetic analyses coupled with ecological niche modelling (ENM) and Bayesian inference (BI) methods to give insight into the structuring of genetic variation of *P. calyculatus* populations.

2 | MATERIALS AND METHODS

2.1 | Study system

Psittacanthus calyculatus is a morphologically variable species that possibly intergrades with *P. schiedeanus* (Kuijt, 2009; Ornelas et al., 2016). Its orange-to-red, hummingbird-pollinated flowers are self-compatible (Azpeitia & Lara, 2006; Díaz Infante, Lara, Arizmendi, Eguarte, & Ornelas, 2016), and its purplish-black, fleshy (one-seed) fruits are consumed by several bird species (Díaz Infante et al., 2016; Lara, Pérez, & Ornelas, 2009). According to Kuijt (2009), it commonly parasitizes *Quercus* along the TMVB, but it has a broad range of hosts (c. 50 host tree species of diverse angiosperm families), including non-native tree species in agricultural landscapes or near cities (Pérez-Crespo, Lara, & Ornelas, 2016 and references therein). Although cross-seed inoculation experiments have shown local adaptation to their hosts (Lara et al., 2009), the broad host

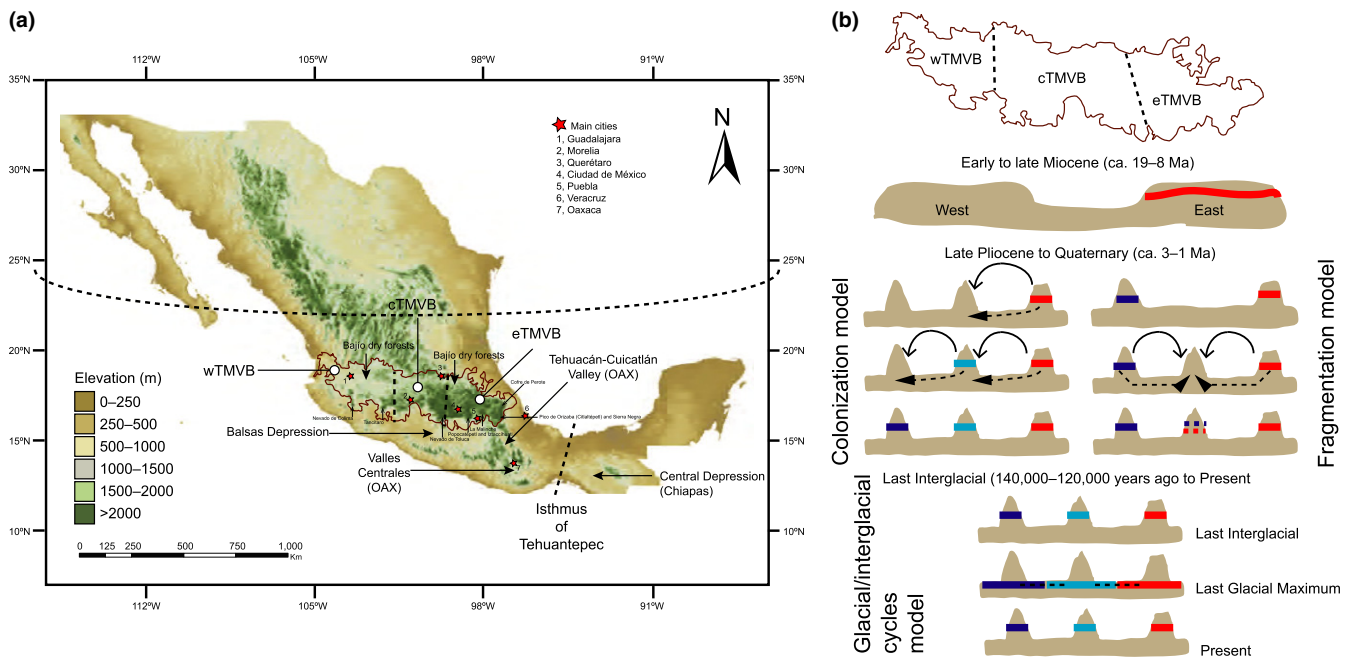


FIGURE 1 (a) Elevation range in metres (m) and location of the Trans-Mexican Volcanic Belt (TMVB). The approximate east-central-west divisions of the TMVB formation are indicated with dashed lines. Main cities and some stratovolcanoes of the TMVB that emerged during the Pleistocene are indicated. (b) Late Miocene to Quaternary scenarios and expected effects of the climate–volcanism interaction are shown according to Mastretta-Yanes et al. (2015). The first three episodes of the TMVB evolution formed highlands where populations of *P. calyculatus* could have differentiated allopatrically, generating the east–west division of sister lineages. The emergence of more recent intermediate volcanoes created continuous highlands in what used to be a geographical barrier, which according to the fragmentation model allowed colonization of these new intermediate habitats and admixture from differentiated east–west sources or a stepping-stone east-to-west colonization and interglacial differentiation according to the colonization model. The glacial/interglacial cycles model poses that the overlap of volcanic episodes created an isolated distribution of suitable conditions for *Psittacanthus calyculatus* advancing into the lowlands during glacial stages, potentially leading to admixture and gene flow and erasing previous patterns of genetic structuring generated during interglacial cycles

range of *P. calyculatus* suggests low host specificity and, consequently, the distribution of genetic variation in this species is unlikely influenced by the distribution of potential host species at a larger geographical scale (Díaz Infante et al., 2016; Ornelas et al., 2016).

2.2 | Samples and DNA sequencing

Leaf tissue samples were collected from 370 individuals on a wide variety of host species in 35 localities (hereafter referred to as populations) covering the species range (Figure 1, Appendix S1: Table S1 of the Supporting Information), spanning from 54 to 2,700 m above sea level. Target sampling populations were chosen based on localities of occurrence from Kuijt (2009), including six populations in each of the eastern (eTMVB), central (cTMVB) and western (wTMVB) areas of the TMVB (Ferrari et al., 2012), and 17 populations from Puebla and Oaxaca south of the TMVB (OAX); most populations collected have an accompanying herbarium voucher (Appendix S1: Table S1). Care was taken to collect only samples from one adult, flowering individual per individual host tree and the individuals present in the same location were treated as a population, ranging from 3 to 23 individuals per population.

The internal transcribed spacer (ITS) region of the nuclear ribosomal DNA (nrDNA) in combination with sequences of *trnL-F*

intergenic spacer from the chloroplast genome (cpDNA) was amplified by PCR and sequenced for 370 individuals. These markers show the appropriate level of variation for mistletoe studies at the species and population levels (e.g. Amico, Vidal-Russell, García, & Nickrent, 2012; Ornelas et al., 2016). As the chloroplast genome is maternally inherited in most angiosperms, cpDNA sequences provide insight into seed-mediated gene flow compared to the nrDNA sequences reflecting a combination of both pollen and seed movement (Ornelas et al., 2016). Primers and protocols for DNA extraction, for PCR reactions and for sequencing the PCR products are described elsewhere (Ornelas et al., 2016). All sequence data were deposited in GenBank (accession nos. ITS: KX640930–KX640946, *trnL-F*: KX640947–KX640960). We additionally included 96 ITS and *trnL-F* sequences of 14 *Psittacanthus* species and 36 sequences of 18 representatives of Loranthaceae tribes downloaded from the GenBank to be used as outgroups (Appendix S1: Table S2).

2.3 | Palaeodistribution modelling and environmental variation

We used ENM (Elith et al., 2011) to predict the distribution of *P. calyculatus* at the Mid-Holocene (MH; c. 6 ka), Last Glacial Maximum

(LGM, c. 20 ka) and Last Interglacial (LIG, c. 130 ka), and to examine whether range expansion/contraction and population connectivity are congruent with the predicted changes in the distribution of temperate forests along the TMVB as suggested by Mastretta-Yanes et al. (2015).

We constructed ENMs and projected onto past climatic conditions with MAXENT 3.3.3e (Phillips, Anderson, & Schapire, 2006) and 19 bioclimatic variables from the WorldClim database (Hijmans, Cameron, Parra, Jones, & Jarvis, 2005) at c. 1 km² spatial resolution. We also obtained data for past climate layers for two MH (2.5 arc-minutes, pixel size c. 21.62 km²) and LGM (2.5 arc-minutes) past conditions based on CCSM4 and MIROC-ESM global models (Braconnot et al., 2007; Hijmans et al., 2005). Coordinates of occurrence data obtained from Kuijt (2009) were assembled and supplemented with our geo-referenced records from field collection. We restricted the dataset to 148 presence records for the analysis where precise coordinates were available. Lastly, we compared the distribution models for the present, MH, LGM and LIG to analyse climatic stability among populations of *P. calyculatus*. Further details and measures of model performance and stability are given in Appendix S1: Methods and Appendix S2: Figures S1–S2.

2.4 | Phylogenetic analysis, divergence time estimation and haplotype relationships

We estimated phylogenetic relationships from the concatenated dataset using BI. We conducted BI analyses using MRBAYES 3.12 (Huelsenbeck & Ronquist, 2001; Ronquist & Huelsenbeck, 2003) on the CIPRES Science Gateway computing cluster (Miller, Pfeiffer, & Schwartz, 2010), with further details in Appendix S1: Methods.

We used a Bayesian approach implemented in BEAST 1.8.4 (Drummond, Suchard, Xie, & Rambaut, 2012) to estimate the phylogenetic relationships among *P. calyculatus* ribotypes and haplotypes and time to most recent common ancestor for lineages related to pre-Pleistocene and Pleistocene events (for a detailed description of our analysis, see Appendix S1: Methods).

To infer genealogical relationships among ribotypes (ITS) and haplotypes (*trnL-F*), statistical parsimony networks for both datasets were constructed using TCS 1.2.1 (Clement, Posada, & Crandall, 2000), with gaps treated as single evolutionary events (*trnL-F*) or missing data (ITS) and a connection limit set to 95%. Loops were resolved following the criteria given by Pfenninger and Posada (2002).

2.5 | Population genetic diversity indices, geographical structure and relationships among populations

Population diversity indices for unordered (h_s , h_T) and ordered haplotypes (v_s , v_T) and differentiation (G_{ST} , N_{ST}) parameters were estimated for each marker using PERMUT 1.0 (Pons & Petit, 1996). Significant differences between N_{ST} and G_{ST} parameters were tested

with 10,000 permutations. If N_{ST} is significantly larger than G_{ST} , this means that two alleles sampled from the same region are phylogenetically more closely related than two alleles sampled from different regions, evidencing the presence of a significant phylogeographical signal in the data (Pons & Petit, 1996). Molecular diversity indices, neutrality tests and pairwise comparisons of F_{ST} values between groups (Appendix S1: Table S1) were calculated using ARLEQUIN 3.01 (Excoffier, Laval, & Schneider, 2005).

Four analyses of molecular variance (AMOVAs; Excoffier, Smouse, & Quattro, 1992) were performed using ARLEQUIN based on pairwise differences to explore population structure along the TMVB, with populations treated as (a) a single group to determine the amount of variation partitioned among and within populations, and (b) grouped into two (TMVB, OAX) or (c) three (wTMVB, cTMVB+eTMVB, OAX) according to the first episodes of TMVB formation or (d) four groups (wTMVB, cTMVB, eTMVB, OAX) resembling the final episode of TMVB formation together with Pleistocene climatic fluctuations (Figure 1, Appendix S1: Table S1). The AMOVAs were performed using the Tamura and Nei model and 16,000 permutations to determine the significance of each AMOVA. Spatial analysis of molecular variance (SAMOVA 1.0; Dupanloup, Schneider, & Excoffier, 2002) was also used to identify clusters of populations that are geographically homogeneous and maximally differentiated (for a detailed description of our analysis, see Appendix S1: Methods).

To estimate the relationships among groups of populations (Figure 1, Appendix S1: Table S1), we used ITS and *trnL-F* sequences for *P. calyculatus* samples and *BEAST (Heled & Drummond, 2010) with the multispecies coalescent model (Appendix S1: Methods).

2.6 | Demographic history

We used mismatch distributions and Bayesian skyline plots (BSP) to assess population expansion and time variation in effective population size (N_e) (Appendix S1: Methods). Note that the spatial population expansion or historical population size changes can be influenced by several sources of error (e.g. sample size, sampling scheme, levels of polymorphism, mutation rates) or by genetic hitchhiking of polymorphism linked to genes under positive selection (e.g. Grant, 2015).

2.7 | Divergence and colonization of the TMVB

To compare scenarios of divergence and colonization history of *P. calyculatus*, we used an approximate Bayesian computation (ABC) approach using DIYABC (Cornuet et al., 2008, 2014) and both ITS and *trnL-F* datasets. Four evolutionary scenarios were constructed considering the haplotype network, AMOVA, SAMOVA and *BEAST results. Although there are numerous possible scenarios of divergence, we considered that these four scenarios represent the close relationships among the groups and the complex patterns of genetic divergence and admixture predicted by both the colonization and glacial/interglacial cycles' models illustrated in Figure 1.



Comparison of scenarios was implemented in DIYABC with 2 million coalescent-based simulated datasets under each evolutionary scenario. For this analysis, we used a prior distribution of mutation rates of 1×10^{-9} – 1×10^{-7} for ITS and 1×10^{-8} – 1×10^{-9} for cpDNA to include those in the literature (Appendix S1: Methods). As the ABC computation jointly samples the mutation rates and effective population sizes, it is often hard to estimate confidently the N_e of populations. Thus, to ensure convergence, we defined a N_e prior with a normal distribution for the OAX population based on previous estimates in *P. schiedeanus* (Ornelas et al., 2016). This normal distribution was set with a mean of 70,000 ($SD = 20,000$), minimum of 10,000 and maximum of 140,000. For all other populations, we used uniform priors with upper bounds that were defined with preliminary ABC runs. Given the absence of independent sources of information on population sizes, these uniform priors can be thought of as uninformative priors. However, defining these priors with very high upper boundaries often leads to the exploration of unrealistic parameter space. Often, initial runs using wide-ranging flat priors lead to simulations that are very far away in parameter space from the observed data. In this context, the upper boundaries of the N_e priors were set in order to obtain simulations that closely resembled the observed data. In any case, we believe these upper boundaries had little effect on the estimations, given that all N_e posterior distributions are skewed toward the lower limit of the prior.

Thus, we used uniform prior distributions (minimum, maximum) for the size of the sampled populations: wTMVB (0, 40,000); cTMVB (0, 50,000); eTMVB (10,000, 100,000). In addition, we used a uniform prior distribution (10,000, 1,200,000) for the ancestral population size (N_a), with the condition $N_a \leq N_e$ OAX. Finally, the prior distribution of the timing of events was set to encompass the time periods of interest and considering a generation time of 11 years: t_1 (100, 10,000); t_2 (100, 10,000); t_3 (1,000, 30,000). To avoid incongruences in the simulated genealogies, we set two conditions on the prior time distributions: $t_1 \leq t_2 < t_3$.

The overall performance of scenarios was evaluated with a principal components analysis in the space of summary statistics on the two million simulated datasets and the observed data (Cornuet et al., 2014). After this pre-evaluation, the posterior probability of scenarios was assessed using a logistic regression procedure on the 1% (20,000) of simulated datasets closest to the observed data (Fontaine et al., 2013). For the best-supported scenario, we used the posterior distributions to simulate 1,000 pseudo-observed datasets in order to evaluate whether this model could successfully reproduce the observed data. We used 1,000 datasets simulated under different scenarios to estimate the posterior predictive error of the analyses and estimate Type I error rates for our selected model (Robert, Cornuet, Marin, & Pillai, 2011). Finally, the posterior probability distributions for demographic and temporal parameters were obtained by local linear regression on the 1% of simulations for the best-supported scenario (5,000) closest to the observed dataset (Cornuet et al., 2008, 2014).

3 | RESULTS

3.1 | Palaeodistribution modelling and environmental variation

The ENMs yielded a good fit for the current geographical distribution of *P. calyculatus* (Figure 2). The performance of the models was high in 20-fold cross-validation of AUC (mean \pm $SD = 0.959 \pm 0.009$). Determination of the threshold probability for predicted presence using the true skill statistic (TSS) resulted in a mean proportion of correctly classified training observations of 0.732 ± 0.073 . The estimated potential distribution of *P. calyculatus* indicates that this species had a relatively unstable distribution range during the last 140,000 years. Predicted present and past models showed some important changes in distribution since LIG, with more stable portions of the predictions in OAX, followed by expansion from LIG to LGM toward the higher TMVB (lower probability applying CCSM than MIROC simulations), and contraction from LGM to MH in northern portions of the region (Figure 2, Appendix S2: Figures S1–S2).

3.2 | Phylogenetic analysis, divergence time estimation and haplotype relationships

The topology of the resulting BI tree confirmed the monophyly of *Psittacanthus* samples ($PP = 1$; Appendix S2: Figure S3). Samples from *Psittacanthus calyculatus* and *P. schiedeanus* form a monophyletic group ($PP = 1$), with genealogical relationships within the ingroup unresolved.

The BEAST analyses placed the diversification of the *Psittacanthus* crown clade as occurring in the Late Miocene (Appendix S2: Figure S4). Although a split between *P. auriculatus* and samples of *P. schiedeanus* and *P. calyculatus* is estimated at 1.77 Ma (95% HPD 2.62–0.68 Ma) with strong support ($PP = 1$), the relationships within the *P. calyculatus/schiedeanus* clade were poorly resolved with diversification of the clade occurring in the Pleistocene (1.28 Ma, 95% HPD 1.81–0.53 Ma; Appendix S2: Figure S4).

The aligned ITS dataset for 334 samples of *P. calyculatus* (559 bp) yielded 21 ribotypes (Table 1). In the ribotype network (Figure 3), one ribotype (R1) was found in 235 of the 334 samples for 33 of the 35 sampled populations and forms the core of the network, from Zacatecas to southern Oaxaca. This widespread and most frequent ribotype (70.4% of the individuals and 97% of the sampled populations) was separated from most other ribotypes by one or two mutations, which were largely singletons. The second most frequent and most widespread ribotype (R16; 64 samples, 19% of all individuals) was found in 19 populations (54% of the sampled populations). Ribotypes R6–R7, R9–R11, R13, R15, R17–R18 and R20 were not singletons and were mostly distributed in Tlaxcala, Puebla and Oaxaca (Figure 3).

The aligned *trnL-F* dataset for 318 samples of *P. calyculatus* (294 bp) yielded 14 haplotypes (Table 1). Statistical parsimony retrieved a well-resolved network (Figure 4), in which the most frequent (136 samples) and widespread haplotype H1 (42.7% of the

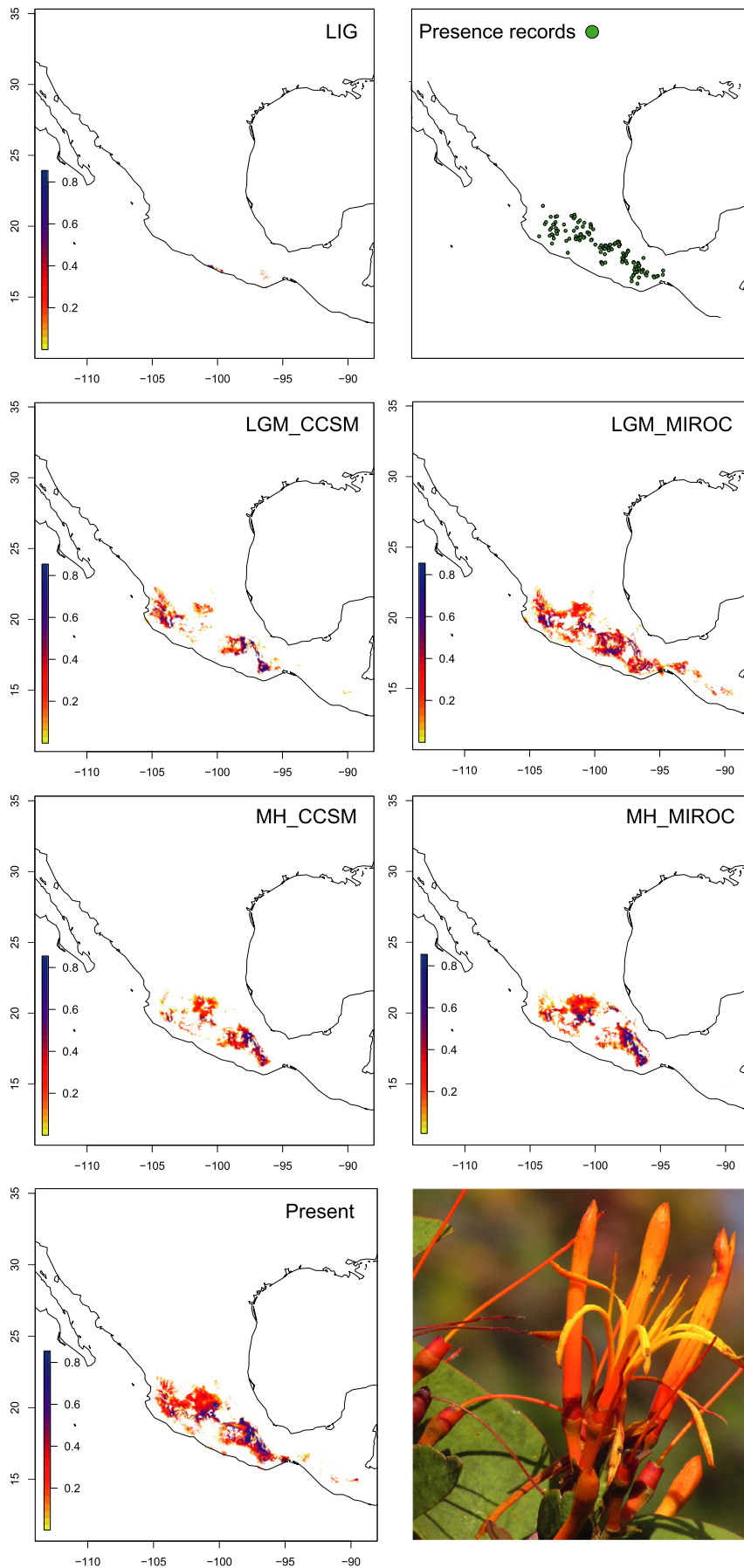


FIGURE 2 Results from the MAXENT analyses showing species distribution models for *Psittacanthus calyculatus* at Last Inter Glacial (LIG, 140–120 ka), Last Glacial Maximum (LGM, CCSM, 21 ka), Last Glacial Maximum (LGM, MIROC, 21 ka), Mid-Holocene (MH, CCSM, 6 ka), Mid-Holocene (MH, MIROC, 6 ka), and at present. The output of MAXENT consists of grid maps with each cell having an index of suitability between 0 and 1. Low values (white to yellow) indicate that the conditions are unsuitable for the species to occur, whereas high values (orange to dark blue) indicate that the conditions are suitable



TABLE 1 Number of genetically analysed samples (*n*) for each molecular marker (ITS and *trnL-F*) and number of distinct ribotypes (R) and haplotypes (H) found in *Psittacanthus calyculatus* individuals sampled, and the number of individuals per ribotype or haplotype in parentheses. Codes are from networks in Figures 3 and 4

Location code	Location	Region	<i>n</i>	ITS ribotype	<i>n</i>	<i>trnL-F</i> haplotype
1	Mexico, Zacatecas, Milpillas	wTMVB	10	R1(7), R16(3)	8	H6(8)
2	Mexico, Zacatecas, El Remolino	wTMVB	10	R1(9), R16(1)	10	H6(10)
3	Mexico, Jalisco, San José de Gracia	wTMVB	17	R1(17)	14	H4(14)
4	Mexico, Jalisco, Pueblo Nuevo	wTMVB	10	R1(8), R16(2)	11	H6(11)
5	Mexico, Jalisco, Gómez Farías	wTMVB	12	R1(12)	12	H6(12)
6	Mexico, Michoacán, La Angostura	wTMVB	9	R1(9)	8	H1(2), H4(6)
7	Mexico, Michoacán, Pátzcuaro	cTMVB	12	R1(11), R2(1)	5	H1(5)
8	Mexico, Michoacán, Maravatío	cTMVB	13	R1(13)	13	H1(13)
9	Mexico, Michoacán, Morelia	cTMVB	10	R1(6), R16(4)	10	H1(10)
10	Mexico, Guanajuato, Acámbaro	cTMVB	10	R1(10)	10	H1(3), H5(7)
11	Mexico, Guanajuato, El Novillero	cTMVB	10	R1(3), R16(7)	10	H1(10)
12	Mexico, Querétaro, Querétaro	cTMVB	10	R1(9), R16(1)	10	H1(10)
13	Mexico, Estado de México, Tenancingo	eTMVB	9	R1(5), R16(4)	10	H1(10)
14	Mexico, Morelos, Cuernavaca	eTMVB	7	R1(5), R16(2)	8	H1(8)
15	Mexico, Morelos, Totolapan	eTMVB	9	R1(3), R16(6)	7	H1(3), H10(4)
16	Mexico, Tlaxcala, Tlaxcala	eTMVB	9	R1(2), R16(1), R17(1), R18(2), R20(2), R21(1)	8	H1(8)
17	Mexico, Tlaxcala, San Luis Teolocholco	eTMVB	10	R1(6), R16(3), R17(1)	8	H1(8)
18	Mexico, Tlaxcala, Nativitas, Sta Agueda	eTMVB	11	R1(11)	10	H1(10)
19	Mexico, Puebla, Rincón de la Monja	OAX	5	R1(5)	6	H13(5), H14(1)
20	Mexico, Puebla, Cerro Tepetroja	OAX	4	R1(4)	5	H7(3), H8(1), H9(1)
21	Mexico, Puebla, Acatepec-Zapotitlán	OAX	5	R1(4), R16(1)	4	H13(4)
22	Mexico, Oaxaca, Cacaotepec, La Presa	OAX	7	R1(3), R16(4), R17(3)	10	H13(10)
23	Mexico, Oaxaca, Santiago Nacaltepec	OAX	-	-	3	H7(3)
24	Mexico, Oaxaca, Tuxtepec, Ixtlán	OAX	8	R1(3), R6(2), R7(3)	6	H11(6)
25	Mexico, Oaxaca, Tuxtepec, Puente Xia	OAX	8	R1(8)	8	H11(8)
26	Mexico, Oaxaca, Oaxaca City	OAX	9	R1(5), R3(1), R4(1), R5(1), R19(1)	9	H11(9)
27	Mexico, Oaxaca, Teotitlán del Valle	OAX	8	R1(6), R16(2)	8	H11(8)
28	Mexico, Oaxaca, Sta María Albarradas	OAX	12	R1(9), R16(3)	13	H1(12), H11(1)
29	Mexico, Oaxaca, Sn Lorenzo Albarradas	OAX	13	R1(10), R16(3)	13	H1(13)
30	Mexico, Oaxaca, Santiago Matatlán	OAX	19	R1(11), R12(1), R16(7)	19	H10(1), H11(18)
31	Mexico, Oaxaca, Sn Baltazar Guelavía	OAX	6	R1(6)	11	H1(10), H12(1)
32	Mexico, Oaxaca, Col. Emiliano Zapata	OAX	6	R1(3), R8(1), R16(2)	6	H3(4), H11(2)
33	Mexico, Oaxaca, Sola de Vega	OAX	11	R1(5), R10(6)	9	H10(9)
34	Mexico, Oaxaca, a Puerto Escondido	OAX	11	R14(1), R16(10)	8	H3(8)
35	Mexico, Oaxaca, Macahuite	OAX	14	R1(6), R9(2), R11(2), R13(2), R15(2)	8	H2(7), H3(1)

Region abbreviations are as follows: TMVB = Trans-Mexican Volcanic Belt; wTMVB = western TMVB; cTMVB = central TMVB; eTMVB = eastern TMVB; OAX = Oaxaca.

individuals and 45.7% of the sampled populations) was mostly retrieved in populations located from the eastern to central portions of the TMVB and south-eastern Oaxaca, followed by haplotypes H4 (20 samples) and H6 (41 samples) exclusively found in the western portion of the TMVB, and haplotypes H7–H14 only retrieved in Oaxaca sites (19–33). Lastly, haplotypes H2 and H3 connected to H1 by one or two steps are haplotypes exclusively found in two sites of Oaxaca (34–35; Figure 4).

3.3 | Population genetic diversity indices, geographical structure and relationships among populations

Differentiation among populations based on ITS variation (mean \pm SE, $G_{ST} = 0.259 \pm 0.0585$) indicated that *P. calyculatus* is genetically subdivided. Genetic diversity across all populations ($h_T = 0.481 \pm 0.0576$; $v_T = 0.481 \pm 0.0899$) was higher than the

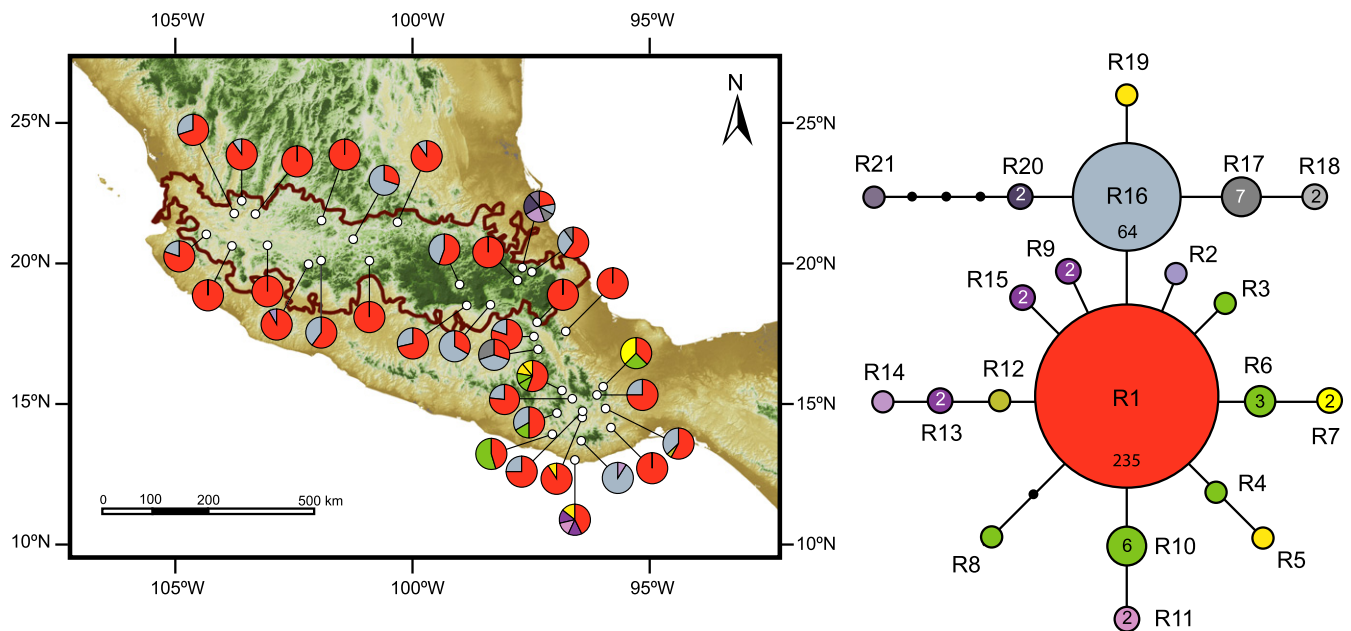


FIGURE 3 Geographical distribution and statistical parsimony network of 21 ITS ribotypes of *Psittacanthus calyculatus* overlaid on a relief map of Mexico. Pie charts represent ribotypes found in each sampling locality

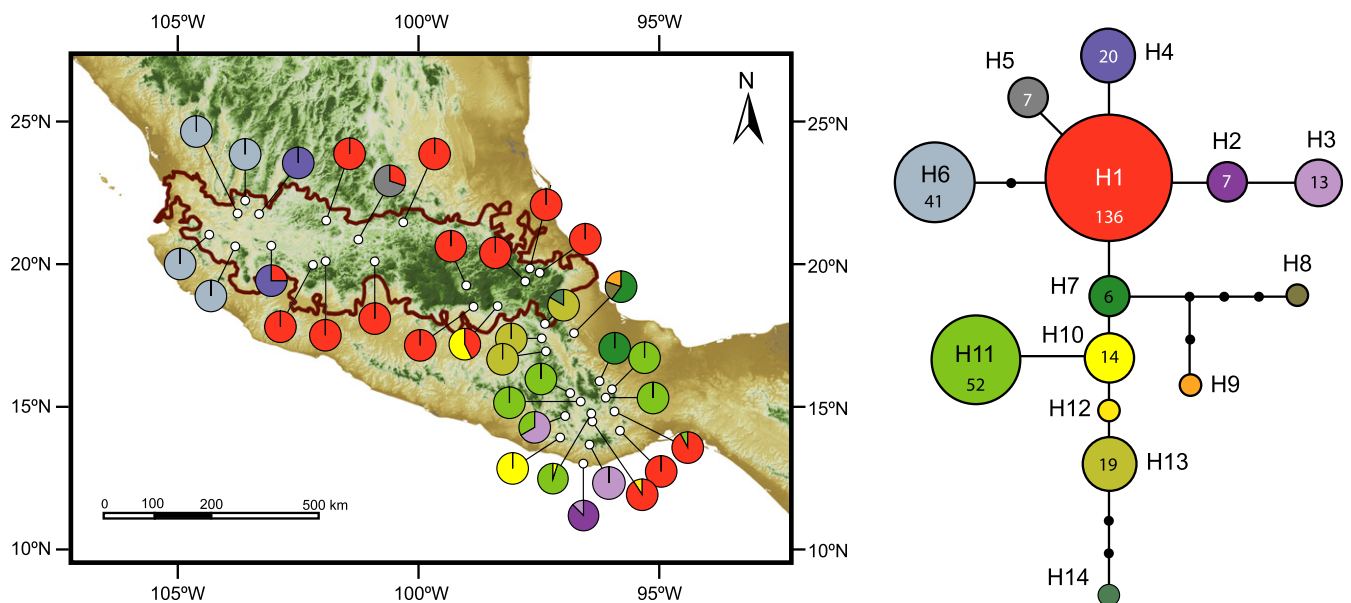


FIGURE 4 Geographical distribution and statistical parsimony network of 14 *trnL-F* haplotypes of *Psittacanthus calyculatus* overlaid on a relief map of Mexico. Pie charts represent haplotypes found in each sampling locality

average within-population value ($h_s = 0.356 \pm 0.0497$; $v_s = 0.347 \pm 0.0656$). PERMUT analysis showed that N_{ST} (0.279 ± 0.0359) was not significantly different ($p > .05$) than G_{ST} , indicating no phylogeographical structuring. Differentiation among populations based on *trnL-F* variation indicated high genetic structuring ($G_{ST} = 0.869 \pm 0.0398$, $N_{ST} = 0.878 \pm 0.0466$), with genetic diversity across all populations ($h_T = 0.811 \pm 0.0495$; $v_T = 0.812 \pm 0.0963$) much higher than the average within-population value ($h_s = 0.106 \pm 0.0337$; $v_s = 0.099 \pm 0.0397$). However, the N_{ST} and G_{ST} values were not statistically different ($p > .05$). Pairwise comparisons of F_{ST} values were mostly low and non-significant for the ITS when groups

of populations were compared, whereas those for *trnL-F* were moderate and significant in all cases (Table 2).

The AMOVA results showed that 75.7% of the genetic variation for ITS and 10% for *trnL-F* was explained by differences within populations when all locations were treated as a single group (Table 3). The AMOVA for the *trnL-F* revealed population structure, with the highest F_{CT} value obtained when populations are grouped into wTMVB, cTMVB+eTMVB and OAX, but for the ITS, these differences were not significant (Table 3), suggesting that seed-mediated dispersal is more limited than pollen-mediated dispersal. When sampling sites are grouped as two or four groups, significant

but smaller proportion of the *trnL-F* variation was attributed to group differences (Table 3). SAMOVA results revealed significant F_{CT} values for groups between $K = 2$ and $K = 10$. For the ITS dataset, the F_{CT} value was highest for $K = 2$ (Table 3). When $K = 3$, F_{CT}

is smaller than $K = 2$, and an additional increase in the number of K led to a dissolution of group structure and single-population groups were formed. For the *trnL-F* dataset, the F_{CT} value was highest for $K = 6$ (Table 3). The six groups were geographically consistent and encompassed three OAX clusters (cluster 1: sites 28–29, 31; cluster 2: sites 20, 23–27, 30; cluster 3: sites 19, 21–22), one cTMVB cluster (sites 7, 9–12), one eTMVB cluster (sites 14–15) + OAX (sites 32–35), and one wTMVB (sites 1–6) + cTMVB (site 8) + eTMVB (sites 13, 16–18) cluster. Nucleotide diversity (π) was low for ITS and low-to-moderate for *trnL-F* datasets (Table 4); cpDNA variation was not correlated with altitude variance among areas (Appendix S2: Figure S5).

The *BEAST tree of multilocus data for differentiation between the wTMVB, cTMVB+eTMVB and OAX clades was the best-supported delimitation hypothesis compared with alternative group assignments (Appendix S2: Figure S6). However, the difference was

TABLE 2 Pairwise comparisons of F_{ST} values of ITS (above the diagonal) and *trnL-F* (below the diagonal) among groups of *Psittacanthus calyculatus* populations

Group	wTMVB	cTMVB	eTMVB	OAX
wTMVB	–	0.0386	0.1002	0.1078
cTMVB	0.4675	–	0.0141	0.0299
eTMVB	0.5470	0.3115	–	0.0101
OAX	0.3421	0.3074	0.3603	–

Significant values at $p < .001$ are shown in bold. Group abbreviations are as follows: wTMVB = western TMVB; cTMVB = central TMVB; eTMVB = eastern TMVB; OAX = Oaxaca.

TABLE 3 Results of AMOVA and SAMOVA models on *Psittacanthus calyculatus* populations with no groups defined a priori (a), and (b) grouped into two groups (TMVB, OAX), (c) grouped into three groups (wTMVB, cTMVB+eTMVB, OAX) according to first stages of dynamic orogenic history of TMBV or (d) four groups (wTMVB, cTMVB, eTMVB, OAX) resembling final stage of orogenic history of TMBV with formation of stratovolcanoes and field lowlands together with Pleistocene climatic fluctuations (Figure 1, Appendix S1: Table S1). (e) SAMOVA $K = 2$ groups for ITS and $K = 6$ groups for *trnL-F*

	ITS					<i>trnL-F</i>				
	df	Sum of squares	Estimated variance	%	Fixation indices	df	Sum of squares	Estimated variance	%	Fixation indices
(a) No groups defined										
Among populations	33	11.746	0.0273	24.32		34	318.24	1.01787	89.96	
Within populations	304	25.858	0.0851	75.68	$F_{ST} = 0.24^{***}$	284	32.28	0.11366	10.04	$F_{ST} = 0.89^{***}$
Total	337	37.604	0.1124			318	350.51	1.13153		
(b) Two groups										
Among groups	1	0.466	0.0005	0.46	$F_{CT} = 0.05$ ns	1	56.77	0.30239	23.65	$F_{CT} = 0.23^{**}$
Among pop. within groups	32	11.280	0.0271	24.03	$F_{SC} = 0.24^{***}$	33	261.47	0.86282	67.47	$F_{SC} = 0.88^{***}$
Within populations	304	25.858	0.0851	75.51	$F_{ST} = 0.24^{***}$	284	32.28	0.11366	8.89	$F_{ST} = 0.91^{***}$
Total	337	37.604	0.1128			318	350.51	1.27888		
(c) Three groups										
Among groups	2	0.534	−0.0012	−1.09	$F_{CT} = −1.09$ ns	2	96.02	0.39727	31.30	$F_{CT} = 0.31^{***}$
Among pop. within groups	31	11.212	0.0281	25.13	$F_{SC} = 0.25^{***}$	32	222.22	0.75829	59.74	$F_{SC} = 0.86^{***}$
Within populations	304	25.858	0.0851	75.97	$F_{ST} = 0.24^{***}$	284	32.28	0.11366	8.96	$F_{ST} = 0.91^{***}$
Total	337	37.607	0.1119			318	350.51	1.26922		
(d) Four groups										
Among groups	3	0.752	−0.0018	−1.63	$F_{CT} = −1.63$ ns	3	96.77	0.33033	26.96	$F_{CT} = 0.27^{**}$
Among pop. within groups	30	10.994	0.0286	25.60	$F_{SC} = 0.25^{***}$	31	221.47	0.78181	63.78	$F_{SC} = 0.87^{***}$
Within populations	304	25.858	0.0850	76.02	$F_{ST} = 0.23^{***}$	284	32.28	0.11366	9.27	$F_{ST} = 0.90^{***}$
Total	337	37.604	0.1118			318	350.51	1.22579		
(e) SAMOVA										
Among groups	1	8.948	0.19838	24.50	$F_{CT} = 0.24^*$	5	1492.87	5.86661	82.34	$F_{CT} = 0.82^{***}$
Among pop. within groups	32	61.288	0.14615	18.05	$F_{SC} = 0.23^{***}$	29	196.19	0.69750	9.79	$F_{SC} = 0.55^{***}$
Within populations	304	141.420	0.46520	57.45	$F_{ST} = 0.42^{***}$	282	158.06	0.56050	7.87	$F_{ST} = 0.92^{***}$
Total	337	211.692	0.80973			316	1847.13	7.12461		

ns, not significant ($p > .05$), $^*p < .01$, $^{**}p < .001$, $^{***}p < .0001$.

TABLE 4 Summary statistics of demographic analysis of *Psittacanthus calyculatus* samples by four groups (wTMVB, cTMVB, eTMVB, OAX) resembling final stage of orogenic history of TMBV with formation of stratovolcanoes and field lowlands together with Pleistocene climatic fluctuations (Figure 1, Appendix 1: Table S1) to infer demographic range expansion. (a) ITS, (b) *trnL-F*

Parameter	wTMVB	cTMVB	eTMVB	OAX
(a) ITS				
N	69	65	55	149
N _H	3	6	9	22
h	0.3069 ± 0.0676	0.5760 ± 0.0647	0.6687 ± 0.0563	0.7606 ± 0.0325
π	0.0000 ± 0.0000	0.0000 ± 0.0002	0.0006 ± 0.0007	0.0013 ± 0.0011
D _T	n.a.	−1.0754	−1.6822*	−1.303
F _S	n.a.	−15.2105***	−10.7414***	−26.9247***
SSD	n.a.	0.00000076	0.0016	0.0053
Hri	n.a.	0.8816	0.4978	0.1047*
(b) <i>trnL-F</i>				
N	63	58	52	146
N _H	3	4	4	13
h	0.4822 ± 0.0459	0.5638 ± 0.0535	0.4155 ± 0.0764	0.7895 ± 0.0209
π	0.0273 ± 0.0143	0.0160 ± 0.0038	0.0102 ± 0.0060	0.0565 ± 0.0280
D _T	2.2439	−0.0003	−0.6109	0.2277
F _S	18.6689	9.2684	5.2226	20.4536
SSD	0.4111***	0.2112	0.1163*	0.6858***
Hri	0.6232	0.3416	0.4422	0.0963

N = number of individuals, N_H = number of ribotypes or haplotypes, h = gene diversity, π = nucleotide diversity, D_T = Tajima's D, F_S = Fu's F_S, SDD = differences in the sum of squares or mismatch distribution, Hri = Harpending's raggedness index. n.a. = not available; *p < .05; ***p < .001. D_T and F_S positive values are indicative of mutation-drift-equilibrium, which is typical of stable populations, and negative values that result from an excess of rare haplotypes indicate that populations have undergone recent expansions, often preceded by a bottleneck. Significantly negative values (at the 0.05 level) reveal in both tests historic demographic expansion events. Significant (p ≤ .05) SSD and Hri values indicate deviations from the sudden expansion model. In bold are shown values that are consistent with demographic expansion.

not very strong, tree nodes showed no strong support (PP < 0.6), and the ESS values were low (< 50).

3.4 | Demographic history

For populations grouped by geography (wTMVB, cTMVB, eTMVB, OAX), neutrality test values were positive (except for cTMVB and eTMVB) and non-significant for the *trnL-F* dataset, indicating demographic stability (Table 4). Negative and significant values for the ITS dataset were detected for cTMVB, eTMVB and OAX (except for Tajima's D value in cTMVB and OAX). In the mismatch distribution, sudden demographic expansion was not rejected for OAX (Hri value) in the ITS, and for wTMVB, eTMVB and OAX (SSD values) in the *trnL-F* (Table 4). The BSPs suggest that the effective population size has not changed in the TMVB and OAX populations over time (Appendix S2: Figure S7).

3.5 | Divergence and colonization of the TMVB

DIYABC analysis indicated that the south-east to north-west colonization model (scenario 2) is the best-supported scenario (Figure 5), with a higher posterior probability value and 95% confidence intervals (PP, 95% CI; scenario 2: 0.983, 0.979–0.986) that did not overlap with those obtained for the other scenarios (scenario 1: 0.016, 0.013–0.019; scenario 3: 0.0004, 0.0003–0.0006; scenario 4:

0.0003, 0.0002–0.0003). Analyses to estimate confidence in scenario choice indicated that Type I error for the best-supported scenario was low (0.124). Under scenario 2, posterior mean parameter estimates indicated that the divergence between OAX and TMVB (t3) occurred 177,100 years before present (CI: 308.00–73.81 ka), assuming an 11-year generation time. In accordance with the colonization model, the splits between eTMVB and cTMVB+wTMVB (t2) and between cTMVB and wTMVB (t1) were dated to 56,000 (104.06–17.93 ka) and 32,010 years before present (72.16–8.77 ka), respectively (Figure 5; Appendix S3: Table S3).

4 | DISCUSSION

4.1 | Mistletoes along the TMVB temperate forests

Our phylogenetic and divergence time estimates indicate that the diversification of *P. calyculatus* is not pre-Pleistocene in origin. This result is discordant with the volcanic origin of mountains along the TMVB and with the idea that the east–west division of the TMVB was a long-standing barrier to dispersal that separated groups of populations. The *BEAST and DIYABC results revealed that the divergence between TMVB and OAX populations occurred 87 and 177 ka, respectively (Figure 5 and Figure S6). These estimates suggest a recent divergence scenario, in which haplotype sharing

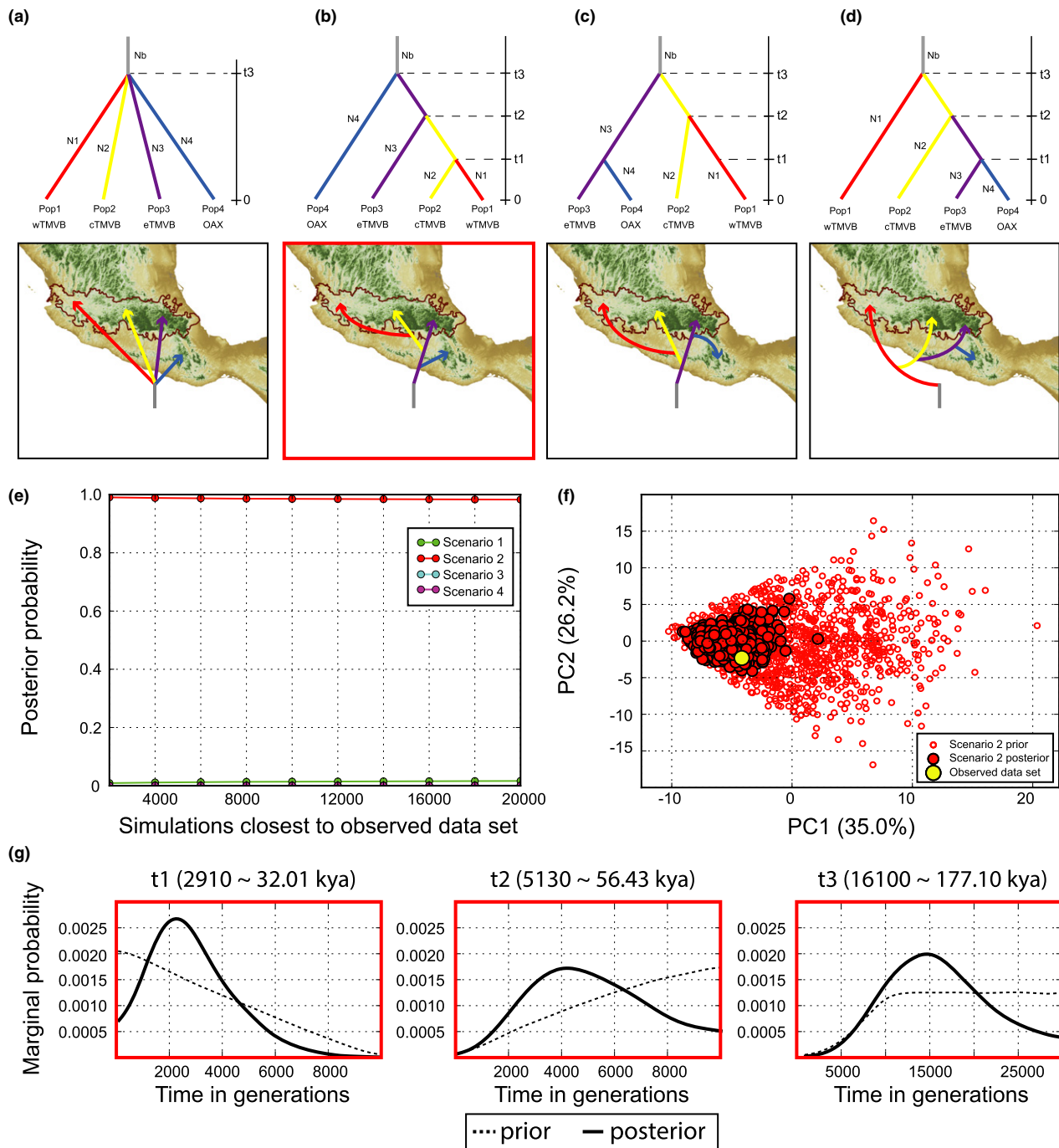


FIGURE 5 Competing demographic scenarios of *Psittacanthus calyculatus* divergence. Four evolutionary scenarios were built and tested considering haplotype network, AMOVAs, SAMOVA and *BEAST results: (a) four populations (Pop1, Pop2, Pop3 and Pop4) that diverged simultaneously from an ancestral population at t3 (scenario 1, null model), which corresponded to the four mistletoe genetic groups, eastern (eTMVB), central (cTMVB) and western (wTMVB) populations along the TMVB, and populations from Puebla and Oaxaca (OAX); (b) colonization model 1 (scenario 2), in which Pop1 (wTMVB) merged with Pop2 (cTMVB) at t1, then both populations merged with Pop3 (eTMVB) at t2 and subsequently with Pop4 (OAX) at t3; (c) isolation split model (scenario 3), in which Pop4 merged with Pop3 at t1, then Pop1 merged with Pop2 at t2, and subsequently both groups of populations merged with Pop4 (OAX) at t3; and (d) colonization model 2 (scenario 4), in which Pop4 merged with Pop3 at t1, then both populations merged with Pop2 at t2 and subsequently with Pop1 at t3. (e) The posterior probability of scenarios was assessed using a weighted logistic regression on the 1% of simulated datasets closest to the observed data and, for the best-supported scenario (scenario 2), (f) a model checking procedure by applying a PCA on test statistic vectors was performed to visualize the fit between the simulated and the observed datasets. Note the large cloud of data from the prior and observed datasets centred on a small cluster from the posterior predictive distribution, suggesting that the best-supported scenario explained the observed data well. (g) Point estimates for temporal parameters (t1–t3) were obtained by local linear regression on the 1% of simulations closest to the observed dataset for the best-supported scenario

between regions results from either retention of ancestral polymorphisms because of insufficient time for lineage sorting, ongoing gene flow across habitats or complete haplotype turnover. The haplotype network, F_{ST} pairwise comparisons, AMOVAs, SAMOVA and *BEAST species delimitation suggest fairly high levels of genetic structuring and the existence of three or more genetic groups, especially when considering the cpDNA data. Altogether these results suggest that changes in the habitat distribution and shifting altitudinal ranges linked to Pleistocene climatic cycles might have fragmented the distribution of *P. calyculatus*.

Inferred patterns of genetic differentiation in *P. calyculatus* appear partially correlated with the ecological differentiation among geographical regions. The pine-oak forests that extend from Jalisco in the west to Veracruz in the east between 2,470 and 2,600 m are surrounded at lower elevations by tropical dry forest to the west (Jalisco dry forests), north-west (Bajío dry forests in the basin of the Río Grande de Santiago and the lower Río Lerma) and south (Balsas dry forests in the basin of the Balsas River) and by shrub land to the north (high basins of the Mexican Plateau, Valley of Mexico and upper reaches of the Río Lerma); the Tehuacán valley with arid tropical shrub and adjacent tropical dry forests lies in the rain shadow valley, adjacent to the pine-oak-dominated portions of the Sierra Madre Oriental to the south-east in Puebla and Tlaxcala states. To the east, the cloud forests of Veracruz and Oaxaca are the transition between the pine-oak forests and the lowland tropical forests along the Gulf of Mexico.

Despite the genetic differentiation of *P. calyculatus* populations observed, widespread ribotypes and haplotypes do occur. The lower variation found in ITS and the presence of widespread ribotypes along with negative values of Tajima's D , Fu's F_s and the results of mismatch distribution suggest effective nuclear gene flow via pollen and recent demographic expansion for populations of *P. calyculatus*, most likely during the LGM. In contrast, the population differentiation of *P. calyculatus* shown by the plastid data suggests that seed flow has been more restricted. Nonetheless, the mechanisms for the observed differentiation call for further analysis.

4.2 | The climate–volcanism interaction along the Trans-Mexican Volcanic Belt

Given the age of the structuring of genetic variation of *P. calyculatus* mistletoes, it is not congruent with geographical isolation resulting from the Miocene TMVB east–west separation (fragmentation model; Mastretta-Yanes et al., 2015; Figure 1). Nor is it congruent with current connectivity along the TMVB of a recently expanded population. The weak genetic structure of *P. calyculatus* populations is more consistent with a scenario of fixed topography and a glacial/interglacial cycle model, involving expansion to the west by stepping-stone colonization and then subsequent interglacial differentiation between populations (colonization model; Mastretta-Yanes et al., 2015; Figure 1, Appendix 2: Figure S2).

This scenario is supported by the fact that haplotypes found in the western *P. calyculatus* collection sites differ from the most

frequent and widely distributed haplotype (H1) by only one mutation and that haplotypes H7–H14 were only retrieved in Oaxaca. Furthermore, the combination of relatively low values of genetic diversity and nucleotide diversity, and the non-significant differences between the N_{ST} and G_{ST} values, indicates rapid population growth from ancestral populations with a small effective population size (Avise, 2000).

Pleistocene climate oscillations influenced the vegetation distribution on the Northern Hemisphere, in which north-to-south contraction and migration of vegetation units seem to predominate in the LGM followed by post-glacial northern expansion and colonization after the glaciers receded (e.g. Hewitt, 1996; Martínez-Meyer & Peterson, 2006). In the Southern Hemisphere, there is no evidence for range shifts toward the north during the LGM and re-colonization of southerly habitats afterward, but rather in situ survival of highland plant species within their extant distribution ranges (e.g. Barros et al., 2015; Jacob, Martínez-Meyer, & Blattner, 2009; Turchetto-Zolet et al., 2016). For *P. calyculatus* in the TMVB, the predictions of ENMs under past LGM climatic conditions and the significant signal of demographic expansion suggest that populations experienced a northward range expansion toward the west of the TMVB and to the lowlands with population connectivity during the LGM, as predicted by the east-to-west colonization and glacial/interglacial cycles models (Mastretta-Yanes et al., 2015). The ENMs predicted major range shifts in suitable habitat for *P. calyculatus* from the LIG to LGM, but minimal east-to-west expansion along the TMVB and contraction of northern areas of the region from LGM to present conditions. Accordingly, we hypothesize that during glacial periods, populations of *P. calyculatus* expanded to the lowlands, where gene flow was extensive, and habitats in which populations had gone extinct during interglacials were probably re-colonized. Throughout interglacial periods, populations fragmented and contracted as they moved up in elevation with the warming climate and genetic divergence commenced.

Interestingly, we found that the number of haplotypes and nucleotide diversity were greater in the OAX population (Table 4). Altitudinal gradients can play an important role in shaping genetic diversity (e.g. Barros et al., 2015; Kingston et al., 2014). Although the diversity of cpDNA haplotypes was not correlated to altitude variance, it is possible that the higher diversity in the *P. calyculatus* cpDNA haplotypes was caused by the higher altitude variance found in the OAX area in addition to the larger stability since the LIG (Appendix S2: Figures S1 and S5).

In conclusion, ENM and phylogeographical evidence both support the unstable distribution of *P. calyculatus* during the last 140,000 years. The ABC analyses strongly supported the scenario of an early split between the OAX and TMVB populations and east-to-west colonization of the TMVB dating back c. 177 and 56 ka, respectively. Genetic evidence coupled with expansion/contraction changes in distribution since LIG indicates that climatic fluctuations throughout the Pleistocene would have altered the distribution of suitable habitat for mistletoes along the TMVB, leading to genetic differentiation of *P. calyculatus* by geographical isolation linked to the effects of the glacial/interglacial cycles and environmental factors, driving genetic differentiation from congeners into more xeric vegetation and the colonization of TMVB from east to west. Further

study using faster molecular markers (e.g. SSRs) should provide finer resolution of genetic structure, detection of processes influenced by short periods of time, and critically important to test hypotheses associated with potential factors that may limit the distribution of these mistletoes (e.g. host and abiotic factors).

ACKNOWLEDGEMENTS

We thank S. Díaz Infante, M. Flores-Herrejón, L. M. García-Feria, A. Langle, C. Lara, H. Martínez-Roldán, F. Rodríguez-Gómez, S. Rodríguez-Mendieta, C. Soberanes and M. Vásquez for field assistance; G. Amico, C. Bárcenas, Y. Licona-Vera and A. Ortiz-Rodríguez for laboratory assistance and data analysis; and C. Lara and Mark Carine for their valuable criticisms and suggestions. Our fieldwork was conducted with the permission of Mexico's Secretaría del Medio Ambiente y Recursos Naturales, Instituto Nacional de Ecología (permit number: SGPA/DGGFS/712/1299/12). This project was funded by competitive grants (grant numbers: 61710, 155686) from the Consejo Nacional de Ciencia y Tecnología (CONACYT; <http://www.conacyt.mx>) and research funds from the Departamento de Biología Evolutiva, Instituto de Ecología, AC (20030/10563) awarded to J.F.O. M.J.P.C. was supported by a doctoral scholarship (365006/248109) and S.R.B. by a postdoctoral fellowship (155686) from CONACYT.

DATA ACCESSIBILITY

DNA sequences: GenBank Accession numbers ITS: KX640930–KX640946, *trnL-F*: KX640947–KX640960. Sequence (FASTA) and MAXENT data available from the Dryad Digital Repository: <https://doi.org/10.5061/dryad.3jq14>. Specimen information: uploaded as Appendix S1: Tables S1 and S2.

REFERENCES

- Amico, G. C., Vidal-Russell, R., García, M. A., & Nickrent, D. L. (2012). Evolutionary history of the South American mistletoe *Tripodanthus* (Loranthaceae) using nuclear and plastid markers. *Systematic Botany*, 37, 218–225.
- Avise, J. C. (2000). *Phylogeography: The history and formation of species*. Cambridge, MA: Harvard University Press.
- Azpeitia, F., & Lara, C. (2006). Reproductive biology and pollination of the parasitic plant *Psittacanthus calyculatus* (Loranthaceae) in central Mexico. *Journal of the Torrey Botanical Society*, 133, 429–438.
- Barros, M. J. F., Silva-Arias, G. A., Fregonezi, J. N., Turchetto-Zolet, A. C., Iganci, J. R. V., Diniz-Filho, J. A. F., & Freitas, L. B. (2015). Environmental drivers of diversity in subtropical highland grasslands. *Perspectives in Plant Ecology, Evolution and Systematics*, 17, 360–368.
- Braconnot, P., Otto-Bliesner, B., Harrison, S., Joussaume, S., Peterchmitt, J. Y., Abe-Ouchi, A., ... Zhao, Y. (2007). Results of PMIP2 coupled simulations of the Mid-Holocene and Last Glacial Maximum –Part 2: Feedbacks with emphasis on the location of the ITCZ and mid- and high latitudes heat budget. *Climate of the Past*, 3, 279–296.
- Bryson, R. W., García-Vázquez, U. O., & Riddle, B. R. (2011). Relative roles of Neogene vicariance and Quaternary climate change on the historical diversification of bunchgrass lizards (*Sceloporus scalaris* group) in Mexico. *Molecular Phylogenetics and Evolution*, 62, 447–457.
- Caballero, M., Lozano-García, S., Vázquez-Selem, L., & Ortega, B. (2010). Evidencias de cambio climático y ambiental en registros glaciales y en cuencas lacustres del centro de México durante el último máximo glacial. *Boletín de la Sociedad Geológica Mexicana*, 62, 359–377.
- Clement, M., Posada, D., & Crandall, K. A. (2000). TCS: A computer program to estimate gene genealogies. *Molecular Ecology*, 9, 1657–1659.
- Cornuet, J. M., Pudlo, P., Veyssier, J., Dehne-García, A., Gautier, M., Leblois, R., ... Estoup, A. (2014). DIYABC v2.0: A software to make approximate Bayesian computation inferences about population history using single nucleotide polymorphism, DNA sequence and microsatellite data. *Bioinformatics*, 30, 1187–1189.
- Cornuet, J. M., Santos, F., Beaumont, M. A., Robert, C. P., Marin, J. M., Balding, D. J., ... Estoup, A. (2008). Inferring population history with DIY ABC: A user-friendly approach to approximate Bayesian computation. *Bioinformatics*, 24, 2713–2719.
- Díaz Infante, S., Lara, C., Arizmendi, M. C., Eguarte, L. E., & Ornelas, J. F. (2016). Reproductive ecology and isolation of *Psittacanthus calyculatus* and *P. auriculatus* mistletoes (Loranthaceae). *PeerJ*, 4, e2491.
- Drummond, A. J., Suchard, M. A., Xie, D., & Rambaut, A. (2012). Bayesian phylogenetics with BEAUti and the BEAST 1.7. *Molecular Biology and Evolution*, 29, 1969–1973.
- Dupanloup, I., Schneider, S., & Excoffier, L. (2002). A simulated annealing approach to define the genetic structure of populations. *Molecular Ecology*, 11, 2571–2581.
- Elith, J., Phillips, S. J., Hastie, T., Dudík, M., Chee, Y. E., & Yates, C. J. (2011). A statistical explanation of MaxEnt for ecologists. *Diversity and Distributions*, 17, 43–57.
- Excoffier, L., Laval, G., & Schneider, S. (2005). Arlequin ver. 3.0: An integrated software package for population genetics data analysis. *Evolutionary Bioinformatics Online*, 1, 47–50.
- Excoffier, L., Smouse, P., & Quattro, J. (1992). Analysis of molecular variance inferred from metric distances among DNA haplotypes: Application to human mitochondrial DNA restriction data. *Genetics*, 131, 479–491.
- Ferrari, L., Orozco-Esquivel, T., Manea, V., & Manea, M. (2012). The dynamic history of the Trans-Mexican Volcanic Belt and the Mexico subduction zone. *Tectonophysics*, 522–523, 122–149.
- Fontaine, M. C., Austerlitz, F., Giraud, T., Labbé, F., Papura, D., Richard-Cervera, S., & Delmotte, F. (2013). Genetic signature of a range expansion and leap-frog event after the recent invasion of Europe by the grapevine downy mildew pathogen *Plasmopara viticola*. *Molecular Ecology*, 22, 2771–2786.
- Gómez-Tuena, A., Orozco-Esquivel, M. T., & Ferrari, L. (2007). Igneous petrogenesis of the Trans-Mexican Volcanic Belt. *Geology of Mexico: Celebrating the centenary of the Geological Society of Mexico* (ed. by S. A. Alaniz-Alvarez and A. F. Nieto-Samaniego). *Geological Society of America Special Papers*, 422, 129–181.
- Grant, W. S. (2015). Problems and cautions with sequence mismatch analysis and Bayesian skyline plots to infer historical demography. *Journal of Heredity*, 106, 333–346.
- Halfpeter, G. (1987). Biogeography of the montane entomofauna of Mexico and Central America. *Annual Review of Entomology*, 32, 95–114.
- Heled, J., & Drummond, A. J. (2010). Bayesian inference of species trees from multilocus data. *Molecular Biology and Evolution*, 27, 570–580.
- Hewitt, G. M. (1996). Some genetic consequences of ice ages, and their role, in divergence and speciation. *Biological Journal of the Linnean Society*, 58, 247–276.
- Hijmans, R. J., Cameron, S. E., Parra, J. L., Jones, P. G., & Jarvis, A. (2005). Very high resolution interpolated climate surfaces for global land areas. *International Journal of Climatology*, 25, 1965–1978.
- Huelsenbeck, J. P., & Ronquist, F. (2001). MRBAYES: Bayesian inference of phylogeny. *Bioinformatics*, 17, 754–755.
- Jacob, S. S., Martínez-Meyer, E., & Blattner, F. R. (2009). Phylogeographic analyses and paleodistribution modeling indicate Pleistocene in situ survival of *Hordeum* species (Poaceae) in Southern Patagonia without genetic or spatial restriction. *Molecular Biology and Evolution*, 26, 907–923.

- Kingston, S. E., Navarro-Sigüenza, A. G., García-Trejo, E. A., Vázquez-Miranda, H., Fagan, W. F., & Braun, M. J. (2014). Genetic differentiation and habitat connectivity across towhee hybrid zones in Mexico. *Evolutionary Ecology*, 28, 277–297.
- Kuijt, J. (2009). Monograph of *Psittacanthus* (Loranthaceae). *Systematic Botany Monographs*, 86, 1–361.
- Lara, C., Pérez, G., & Ornelas, J. F. (2009). Provenance, guts, and fate: Field and experimental evidence in a host-mistletoe-bird system. *Ecology*, 16, 399–407.
- Lozano-García, S., Sosa-Nájera, S., Sugiura, Y., & Caballero, M. (2005). 23,000 yr of vegetation history of the Upper Lerma, a tropical high-altitude basin in Central Mexico. *Quaternary Research*, 64, 70–82.
- Martínez-Meyer, E., & Peterson, A. T. (2006). Conservatism of ecological niche characteristics in North American plant species over the Pleistocene-to-Recent transition. *Journal of Biogeography*, 33, 1779–1789.
- Mastretta-Yanes, A., Moreno-Letelier, A., Piñero, D., Jorgensen, T. H., & Emerson, B. C. (2015). Biodiversity in the Mexican highlands and the interaction of geology, geography and climate within the Trans-Mexican Volcanic Belt. *Journal of Biogeography*, 42, 1586–1600.
- Mastretta-Yanes, A., Zamudio, S., Jorgensen, T. H., Arrigo, N., Alvarez, N., Piñero, D., & Emerson, B. C. (2014). Gene duplication, population genomics, and species-level differentiation within a tropical mountain shrub. *Genome Biology and Evolution*, 6, 2611–2624.
- McCormack, J. E., Heled, J., Delaney, K. S., Peterson, A. T., & Knowles, L. L. (2011). Calibrating divergence times on species trees versus gene trees: Implications for speciation history of *Aphelocoma* jays. *Evolution*, 65, 184–202.
- Miller, M. A., Pfeiffer, W., & Schwartz, T. (2010). *Creating the CIPRES Science Gateway for inference of large phylogenetic trees*. Proceedings of the Gateway Computing Environments Workshop (GCE), 14 November 2010, New Orleans, LA, pp. 1–8. Washington, DC: Institute of Electrical and Electronics Engineers (IEEE), 2010.
- Ornelas, J. F., Gándara, E., Vázquez-Aguilar, A. A., Ramírez-Barahona, S., Ortiz-Rodríguez, A. E., González, C., ... Ruiz-Sánchez, E. (2016). A mistletoe tale: Postglacial invasion of *Psittacanthus schiedeana* (Loranthaceae) to Mesoamerican cloud forests revealed by molecular data and species distribution modeling. *BMC Evolutionary Biology*, 16, 78.
- Ornelas, J. F., González, C., Espinosa de los Monteros, A., Rodríguez-Gómez, F., & García-Ferri, L. M. (2014). In and out of Mesoamerica: Temporal divergence of *Amazilia* hummingbirds predates the orthodox account of the completion of the Isthmus of Panama. *Journal of Biogeography*, 41, 168–181.
- Parra-Olea, G., Windfield, J. C., Velo-Antón, G., & Zamudio, K. R. (2012). Isolation in habitat refugia promotes rapid diversification in a montane tropical salamander. *Journal of Biogeography*, 39, 353–370.
- Pérez-Crespo, M. J., Lara, C., & Ornelas, J. F. (2016). Uncorrelated mistletoe infection patterns and mating success with local host specialization in *Psittacanthus calyculatus* (Loranthaceae). *Evolutionary Ecology*, 30, 1061–1080.
- Pfenniger, M., & Posada, D. (2002). Phylogeographic history of the land snail *Candidula unifasciata* (Helicellinae, Stylommatophora): Fragmentation, corridor migration, and secondary contact. *Evolution*, 56, 1776–1788.
- Phillips, S. J., Anderson, R. P., & Schapire, R. E. (2006). Maximum entropy modeling of species geographic distributions. *Ecological Modelling*, 190, 231–259.
- Pons, O., & Petit, R. J. (1996). Measuring and testing genetic differentiation with ordered versus unordered alleles. *Genetics*, 144, 1237–1245.
- Robert, C. P., Cornuet, J. M., Marin, J. M., & Pillai, N. S. (2011). Lack of confidence in approximate Bayesian computation model choice. *Proceedings of the National Academy of Sciences USA*, 108, 15112–15117.
- Rodríguez-Gómez, F., & Ornelas, J. F. (2015). At the passing gate: Past introgression in the process of species formation between *Amazilia violiceps* and *A. viridifrons* hummingbirds along the Mexican Transition Zone. *Journal of Biogeography*, 42, 1305–1318.
- Ronquist, F., & Huelsenbeck, J. (2003). MrBayes 3: Bayesian phylogenetic inference under mixed models. *Bioinformatics*, 19, 1572–1574.
- Ruiz-Sánchez, E., & Ornelas, J. F. (2014). Phylogeography of *Liquidambar styraciflua* (Altingiaceae) in Mesoamerica: Survivors of a Neogene widespread temperate forest (or cloud forest) in North America? *Ecology and Evolution*, 4, 311–328.
- Ruiz-Sánchez, E., & Specht, C. D. (2013). Influence of the geological history of the Trans-Mexican Volcanic Belt on the diversification of *Nolina parviflora* (Asparagaceae: Nolinoideae). *Journal of Biogeography*, 40, 1336–1347.
- Turchetto-Zolet, A. C., Salgueiro, F., Turchetto, C., Cruz, F., Veto, N. M., Barros, M. J. F., ... Margis, R. (2016). Phylogeography and ecological niche modelling in *Eugenia uniflora* (Myrtaceae) suggest distinct vegetational responses to climate change between the southern and the northern Atlantic Forest. *Botanical Journal of the Linnean Society*, 182, 670–688.
- Vázquez-Selem, L., & Heine, K. (2011). *Late Quaternary Glaciation in Mexico*. In J. Ehlers, P. L. Gibbard, & P. Hughes (Eds.), *Quaternary glaciations – extent and chronology – a closer look* (pp. 849–861). Amsterdam: Elsevier.
- Velo-Antón, G., Parra, J. L., Parra-Olea, G., & Zamudio, K. R. (2013). Tracking climate change in a dispersal-limited species: Reduced spatial and genetic connectivity in a montane salamander. *Molecular Ecology*, 22, 3261–3278.

BIOSKETCH

María José Pérez Crespo is broadly interested in ecology and evolution of plants. She began this study as part of her doctoral dissertation in the Ornelas Lab at INECOL. This working group is a collaboration to test ideas about the ecology and evolutionary history of *Psittacanthus* mistletoes in Mesoamerica.

Author contributions: M.J.P.C. and J.F.O. conceived the ideas and framework for the study; M.J.P.C., A.G.R., E.R.S., A.A.V.A. and S.R.B. collected the data and were involved in obtaining the molecular data; M.J.P.C., J.F.O. and S.R.B. analysed the data; J.F.O. drafted the manuscript and led the writing and all other authors contributed to revisions. All authors read and approved the final manuscript.

SUPPORTING INFORMATION

Additional Supporting Information may be found online in the supporting information tab for this article.

How to cite this article: Pérez-Crespo MJ, Ornelas JF, González-Rodríguez A, Ruiz-Sánchez E, Vázquez-Aguilar AA, Ramírez-Barahona S. Phylogeography and population differentiation in the *Psittacanthus calyculatus* (Loranthaceae) mistletoe: a complex scenario of climate–volcanism interaction along the Trans-Mexican Volcanic Belt. *J Biogeogr.* 2017;00:1–14. <https://doi.org/10.1111/jbi.13070>